

Article

# Effect of Short-Circuit Faults in the Back-to-Back Power Electronic Converter and Rotor Terminals on the Operational Behavior of the Doubly-Fed Induction Generator Wind Energy Conversion System

Dimitrios G. Giaourakis <sup>†,\*</sup> and Athanasios N. Safacas <sup>†</sup>

Electromechanical Energy Conversion Laboratory, Electrical and Computer Engineering Department, University of Patras, University Campus, Rion-Patras 26504, Greece;

E-Mail: a.n.safacas@ece.upatras.gr

<sup>†</sup> These authors contributed equally to this work.

\* Author to whom correspondence should be addressed; E-Mail: dgkiaourakis@ece.upatras.gr; Tel.: +30-261-099-7351.

Academic Editor: David Mba

Received: 30 June 2014 / Accepted: 30 January 2015 / Published: 27 February 2015

---

**Abstract:** This paper deals with the operational behavior of the Doubly-Fed Induction Generator Wind Energy Conversion System under power electronic converter and rotor terminals faulty conditions. More specifically, the effect of the short-circuit fault both in one IGBT of the back-to-back power electronic converter and in rotor phases on the overall system behavior has been investigated via simulation using a system of 2 MW. Finally, the consequences of these faults have been evaluated.

**Keywords:** doubly-fed induction generator (DFIG); short-circuit fault; simulation; wind energy conversion system

---

## 1. Introduction

In last decades, the so-called “renewable or green energies” have gained the worldwide community interest, because of the increasing demand of electric power and the urgent need to reduce the dependence on fossil fuels. Renewable Energy Sources (RES) occupied a large share of installed



of this, the most works deal with open-circuit faults in the back-to-back power electronic converter. More specifically, open-circuits—mainly due to misfiring pulses—in one or in two IGBTs of the Rotor Side Converter (RSC) or Grid Side Converter (GSC) have been considered and fault detection methods have been proposed [14–17]. Finally, a start-up procedure using zero-crossing method for grid synchronization has been studied in [18].

In this work based on a developed model of the whole DFIG-WECS, the system behavior has been studied using the software Matlab/Simulink under faulty situations. More specifically, short-circuit faults in both the back-to-back converter (F1, F2) and rotor terminals (F3) are investigated in typical wind speed (supersynchronous mode) (Figure 1). The consequences of these strong conditions have been studied and critical conclusions about DFIG operational behavior have been obtained. The contribution of this paper is detailed analysis of the main operational system variables offering quantitative and qualitative information at strong dynamic conditions.

## 2. System Basic Operational Principles

The DFIG-WECS (Figure 1) consists of an asynchronous machine and a back-to-back power converter, which is established in the rotor. The asynchronous machine is always operated as a generator and its stator is always connected to the grid. This system has the capability to operate in both subsynchronous and supersynchronous mode. This can be achieved via power flow in both directions. That is why the bi-directional topology of AC/DC/AC converter is used. The rotor electrical power  $P_r$  is only a fraction of stator active power output  $P_s$  ( $P_r = -sP_s$ ). During supersynchronous operation,  $P_r$  is transmitted to DC link capacitor and tends to raise the DC voltage. In subsynchronous speed operation,  $P_r$  is taken out of the DC bus capacitor  $C$  and tends to decrease the DC link voltage.

As far as the back-to-back converter topology is concerned, it consists of two individual and fully-controlled power converters (SPWM technique) with Insulated-Gate Bipolar Transistors (IGBTs). These converters are responsible for the independent control of system's active and reactive power. More specifically, Rotor Side Converter (RSC) is used to control generator active and reactive power and on the other hand Grid Side Converter (GSC) is used to succeed power factor correction and keep the DC link voltage steady at an appropriate value [19]. Furthermore, RSC acts as a PWM rectifier during the machine working in supersynchronous mode and as an inverter during subsynchronous mode, while GSC operates vice versa.

## 3. DFIG Simulation Model

A 2 MW DFIG-WECS model has been developed and simulated in the environment of Matlab/Simulink software for the purposes of this paper [19]. In this section the mathematical description and the implementation of this model in Matlab/Simulink and also its parameter values are presented.

### 3.1. Grid Model

For grid simulation a three phase programmable voltage source has been used. Grid and transformer parameter values are in Table 1.

**Table 1.** Grid and transformer parameter values.

Parameter	Values
$V_{\text{grid}}$ (rms)	20 kV
Frequency	50 Hz
$R_{\text{grid}}/L_{\text{grid}}/\text{Transformer Nominal Power}$	0.008 $\Omega$ /0.001 $\Omega$ /2.5 MVA
Transformer ratio	20 kV/690 V

### 3.2. Wind Turbine Aerodynamics

A wind turbine converts the wind power to mechanical (kinetic) power. The mechanical power  $P_m$  is given by the following equation:

$$P_m = \frac{1}{2} \rho \pi R^3 v_w^3 \frac{C_p(\lambda, \beta)}{\lambda} \quad (1)$$

where  $\rho$  the air density ( $\text{kg/m}^3$ ),  $R$  the wind turbine rotor radius (m),  $v_w$  the equivalent wind speed (m/s),  $\beta$  the pitch angle of rotor (deg),  $C_p$  the power coefficient with its maximum value at 0.59 (Betz limit) and  $\lambda$  is the tip speed ratio given by the following equation:

$$\lambda = \frac{\omega_m R}{v_w} \quad (2)$$

where  $\omega_m$  is the wind turbine rotor speed (rad/s).

The power coefficient  $C_p$  is given by the following equation [19,20]:

$$C_p(\lambda, \beta) = 0.22 \left( \frac{116}{\lambda_t} - 0.4\beta - 5 \right) \exp\left( \frac{-12.5}{\lambda_t} \right) \left. \vphantom{C_p(\lambda, \beta)} \right\} \quad (3)$$

$$\frac{1}{\lambda_t} = \frac{1}{\lambda + 0.08\beta} - \frac{0.035}{\beta^3 + 1}$$

One can see that  $C_p$  is a function of pitch angle  $\beta$  and the tip speed ratio  $\lambda$ . In a given value of  $\beta$ , there is an optimum value for  $\lambda$ , namely  $\lambda_{opt}$  that gives the maximum  $C_p$ . All these values can be calculated by the wind turbine characteristic power curve. Generally, the wind turbines are designed to operate at maximum  $C_p$ . The wind turbine block diagram and parameter values are shown in Figure 2 and Table 2, respectively.

**Table 2.** Wind turbine parameter values.

Parameter	Values
$P_{\text{nom}}$	2 MW
$R$	32.5 m
Nominal wind speed	12 m/s
Cut-in speed	3.5 m/s
Cut-out speed	25 m/s
$\beta_{\text{min}}/\beta_{\text{max}}$	0°/30°
$\beta'$	10°

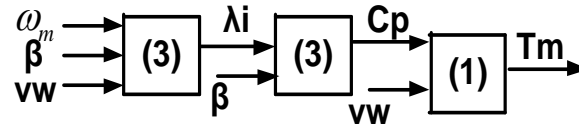


Figure 2. Wind turbine 1.

The pitch angle  $\beta$  is zero when  $v_w \leq v_{w, nom}$ , while it is defined by the pitch system when  $v_w > v_{w, nom}$ . The mathematical equation, which describes the pitch control system, is:

$$\dot{\beta} = \frac{1}{\tau} (\beta_{ref} - \beta) \tag{4}$$

and the corresponding block diagram is in Figure 3 [19].

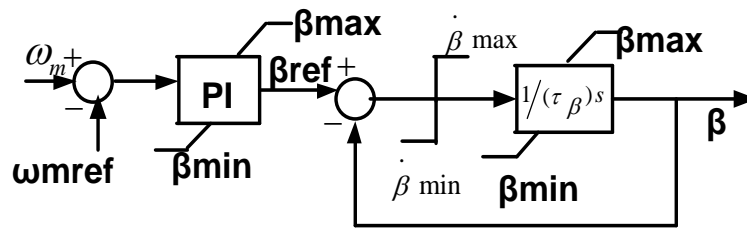


Figure 3. Pitch control.

### 3.3. Asynchronous Generator Model

The asynchronous generator model has been described by the following well-known dynamical equations in d-, q-synchronous reference frame and the parameter values are given in Table 3:

$$\left. \begin{aligned} u_{ds} &= R_s \cdot i_{ds} - \omega_e \lambda_{qs} + \frac{d\lambda_{ds}}{dt} & u_{dr} &= R_s \cdot i_{dr} + \frac{d\lambda_{dr}}{dt} - (\omega_e - \omega_r) \lambda_{qr} \\ u_{qs} &= R_s \cdot i_{qs} + \omega_e \lambda_{ds} + \frac{d\lambda_{qs}}{dt} & u_{qr} &= R_s \cdot i_{qr} + \frac{d\lambda_{qr}}{dt} + (\omega_e - \omega_r) \lambda_{dr} \end{aligned} \right\} \tag{5}$$

$$\left. \begin{aligned} \lambda_{ds} &= (L_{s\sigma} + L_m) i_{ds} + L_m i_{dr} & \lambda_{dr} &= (L_{r\sigma} + L_m) i_{dr} + L_m i_{ds} \\ \lambda_{qs} &= (L_{s\sigma} + L_m) i_{qs} + L_m i_{qr} & \lambda_{qr} &= (L_{r\sigma} + L_m) i_{qr} + L_m i_{qs} \end{aligned} \right\} \tag{6}$$

where  $u_{ds}, u_{qs}, u_{dr}, u_{qr}, i_{ds}, i_{qs}, i_{dr}, i_{qr}, \lambda_{ds}, \lambda_{qs}, \lambda_{dr}, \lambda_{qr}$ , are voltages (V), currents (A) and flux linkages (Wb) of the stator and rotor in d- and q-axis,  $R_s$  is the resistance of the stator windings [ $\Omega$ ],  $L_s, L_r, L_m$ , are the stator, rotor and mutual inductances (H),  $L_{r\sigma}, L_{s\sigma}$  the stator and rotor leakage inductances (H) and  $\omega_{sl} = \omega_e - \omega_r$  is the speed of the reference frame (rad/s). The stator-side and rotor-side active and reactive power are, respectively:

$$\left. \begin{aligned} P_s &= \frac{3}{2}(u_{ds}i_{ds} + u_{qs}i_{qs}) \\ P_r &= \frac{3}{2}(u_{dr}i_{dr} + u_{qr}i_{qr}) \end{aligned} \right\} \left. \begin{aligned} Q_s &= \frac{3}{2}(u_{qs}i_{ds} - u_{ds}i_{qs}) \\ Q_r &= \frac{3}{2}(u_{qr}i_{dr} - u_{dr}i_{qr}) \end{aligned} \right\} \quad (7)$$

**Table 3.** Generator parameter values.

Parameter	Values
P <sub>nom</sub>	2 MW
Stator voltage	690 V
Nominal frequency	50 Hz
R <sub>s</sub>	0.0108 pu
R <sub>r</sub>	0.0121 pu
L <sub>sσ</sub>	0.102 pu
L <sub>rσ</sub>	0.11 pu
L <sub>m</sub>	3.362 pu

### 3.4. Rotor Side Converter Control Model

The control strategy that has been implemented is Flux Oriented Control (FOC) in synchronous reference frame (Figure 4) and the control equations (using PI controllers) are [19]:

$$\left. \begin{aligned} V_{dr}^* &= k_P(i_{dr}^* - i_{dr}) + k_I \int (i_{dr}^* - i_{dr}) dt - \omega_{sl} \sigma L_r i_{qr} \\ V_{qr}^* &= k_P(i_{qr}^* - i_{qr}) + k_I \int (i_{qr}^* - i_{qr}) dt + \omega_{sl} \left( (L_m \Psi_{ds} / L_s) + L_r \sigma i_{dr} \right) \end{aligned} \right\} \quad (8)$$

where  $\sigma = 1 - (L_m^2 / L_r L_s)$ ,  $k_P$ ,  $k_I$  are PI controllers gains,  $i_{dr}^* = \lambda_{ds} / L_m$ ,  $i_{qr}^* = \frac{T_e^*}{\lambda_{ds}} \left( -\frac{2L_s}{3pL_m} \right)$  and  $p$  is the number of pole pairs.

### 3.5. Grid Side Converter Control Model

The control strategy that has been implemented in this work is Grid Voltage Oriented control in synchronous reference frame (Figure 5) and the control equations (using PI controllers) are [19]:

$$\left. \begin{aligned} V_{df}^* &= -k_{Pgsc} (i_{df}^* - i_{df}) - k_{Igsc} \int (i_{df}^* - i_{df}) dt + \omega_e L_f i_{qf} + V_{dg} \\ V_{qf}^* &= -k_{Pgsc} (i_{qf}^* - i_{qf}) - k_{Igsc} \int (i_{qf}^* - i_{qf}) dt - \omega_e L_f i_{df} \end{aligned} \right\} \quad (9)$$

$$\left. \begin{aligned} i_{df}^* &= k_{Pdc} (V_{dc}^* - V_{dc}) + k_{Idc} \int (V_{dc}^* - V_{dc}) dt \\ i_{qf}^* &= k_{PQ} (Q_g^* - Q_g) + k_{IQ} \int (Q_g^* - Q_g) dt \end{aligned} \right\} \quad (10)$$

where  $k_{Pgsc}$ ,  $k_{Igsc}$ ,  $k_{Pdc}$ ,  $k_{Idc}$ ,  $k_{PQ}$ ,  $k_{IQ}$  are PI controllers gains (reactive power and DC link voltage regulators),  $V_{dc}^* = 1200$  V and  $Q_g^* = 0$ .



#### 4. DFIG Behavior Under Short-Circuit Faults

Using the above Matlab/Simulink models, the following cases of faults are analyzed.

##### 4.1. Short-Circuit in One IGBT of the RSC (F1)

The facts that could cause short-circuit in an IGBT are the following [21]:

- (a) a wrong voltage in IGBT gate, which may occurred because of driver circuit malfunction, auxiliary power supply failure, or rapid change of voltage ( $du/dt$ );
- (b) an inherent failure, which may occurred due to an overvoltage/avalanche stress or temperature overshoot.

In this section the DFIG behavior under fault (F1)—Figure 1—is studied. DFIG has been operated in supersynchronous mode ( $n_r = 1800 \text{ rpm} > n_s = 1500 \text{ rpm}$ —Synchronous speed) and at  $t = 4 \text{ s}$  a short-circuit occurred in T1 (upper IGBT, phase a). During the simulation the switching operation of the other switches has not been changed (Rotor phase current  $i_{ra}$ , currents through IGBT (1)—IRT1—and IGBT (4)—IRT4, that have been affected by (F1), are shown in Figure 6, where one can see that very high peak values come up. So, IGBTs breakdown is possible). The protection system has been considered not to be activated and the system has reached in a steady faulty state. According to the simulation results one can see in Figures 7–14 that (F1) has very severe consequences in the operational behavior of the whole system, because of the high current values and great torque oscillations. Initially, a very significant transient phenomenon occurs, which lasts for a long time (from  $t = 4 \text{ s}$  to  $t = 12 \text{ s}$ ). A pulsating torque ( $t_e$ ) has been caused (Figure 7) with great low frequency oscillations and has as a result severe vibration on the mechanical part of the system (turbine-generator-gearbox) and maybe total breakdown of the system. Rotor speed  $n_r$  (rpm) (Figure 8) increases to 2100 rpm (pitch control could be possibly activated, but due to the fact that it consists of mechanical parts, it has high time constant). Then, it oscillates about synchronous speed and finally decreases at 1555 rpm (with oscillations  $\pm 40 \text{ rpm}$ ). In addition, pulsations appear in stator active power, which is no more regulated and this could cause problems to the grid. Figure 9 shows that (F1) has a high effect on the dc link voltage as it decreases significantly. As depicted in Figure 10, DFIG draws 3 pu reactive power from the grid for a time period of 2.5 s and finally oscillates about 1.5 pu. Both rotor (Figure 11) and stator (Figure 12) currents are affected greatly because of (F1). More specifically, a dc component and very high peak values appear in rotor currents—Approximately four times the nominal value during the transient condition and 1.3 times after system equilibration, while stator currents get high values. The dc component worsens the current stress of the healthy converter switches (especially in supersynchronous mode). However, rotor windings and the converter switches could be damaged during the transient state. Finally, in Figures 13 and 14 one can see that (F1) causes high peak values (3.5–4 times the nominal value) and oscillations in both GSC line currents  $I_{gabc}$  and grid phase currents  $I_{gridabc}$  that will result grid disturbances.

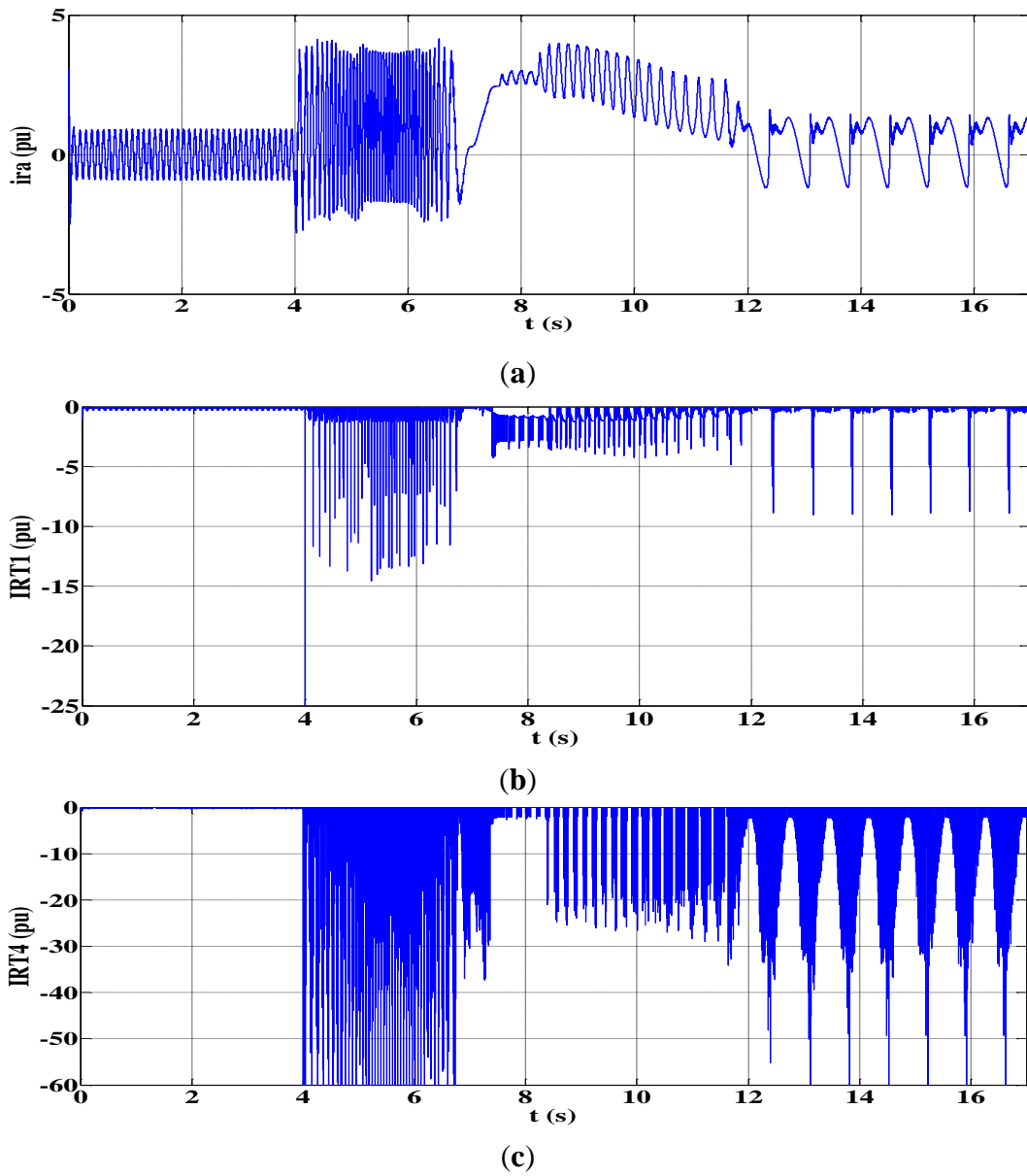


**Figure 6.** Waveforms of the characteristic variables of the RSC: (a) Rotor phase current  $i_{ra}$ , (b) Current through IGBT (1), (c) Current through Insulated Gate Bipolar transistor (IGBT) (4) (short-circuit happens at  $t = 4$  s for all waveforms).

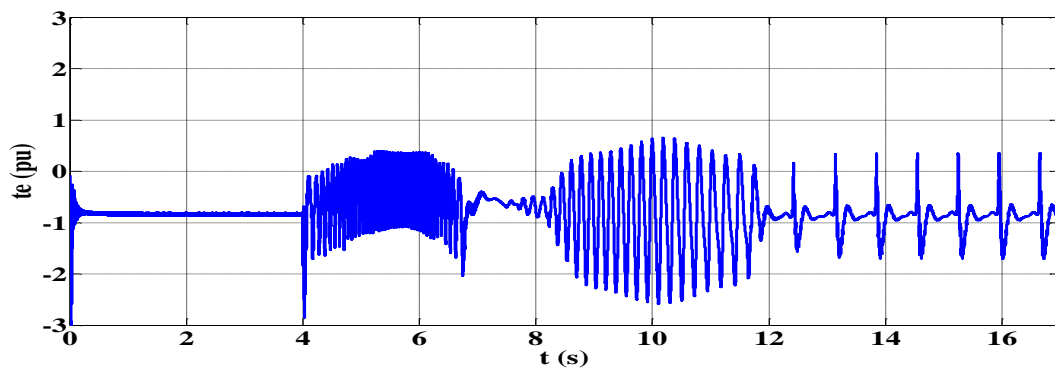


**Figure 7.** Electromagnetic torque (short-circuit happens at  $t = 4$  s).

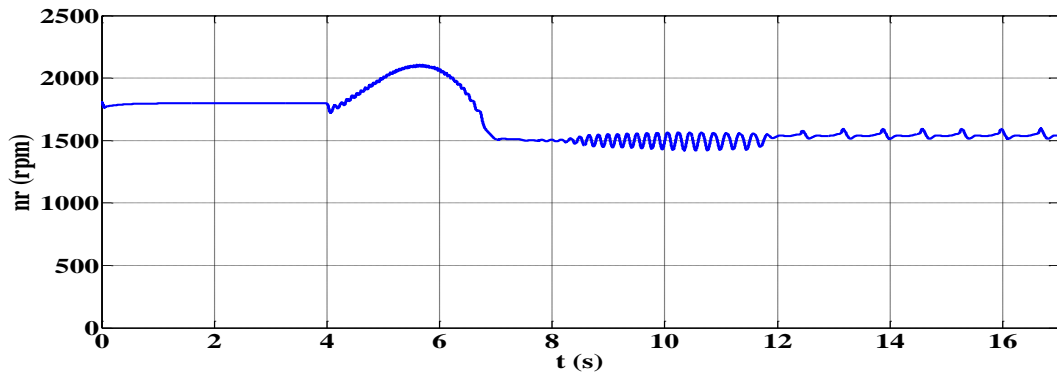


Figure 8. Rotor speed  $n_r$  (short-circuit happens at  $t = 4$  s).

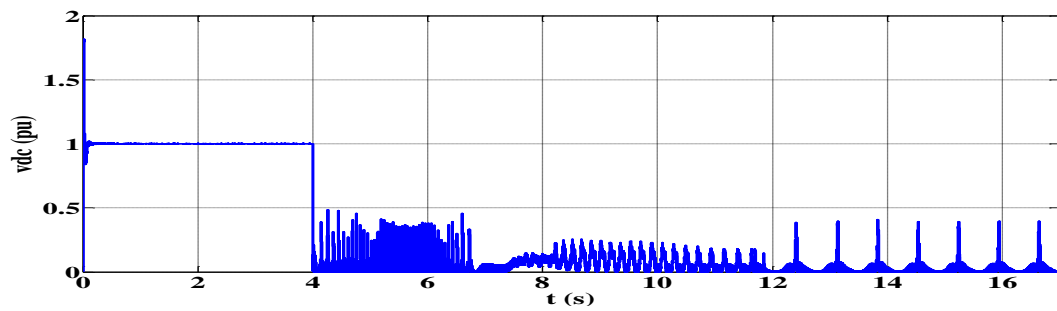


Figure 9. DC link voltage (short-circuit happens at  $t = 4$  s).

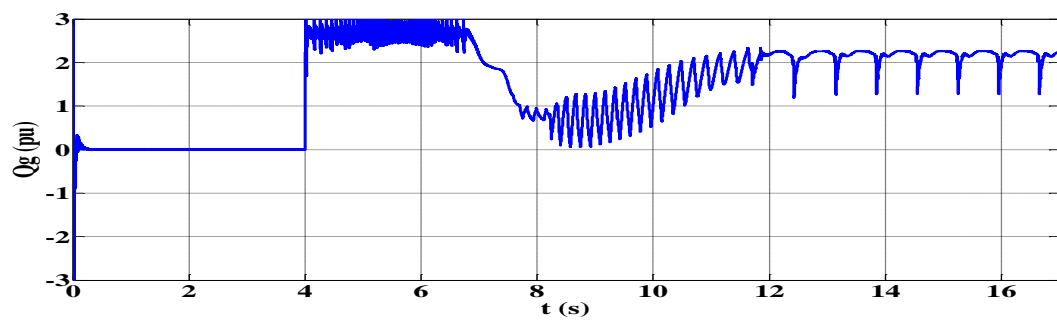


Figure 10. Doubly-Fed Induction Generator (DFIG) reactive power (short-circuit happens at  $t = 4$  s).

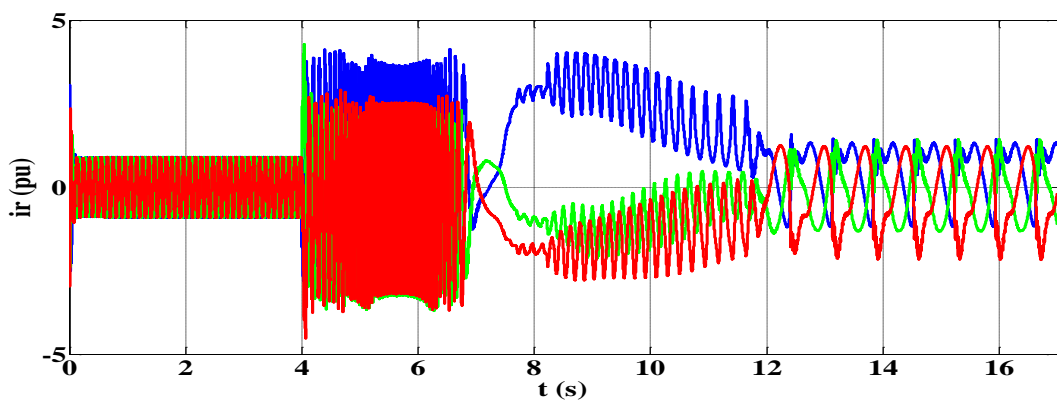
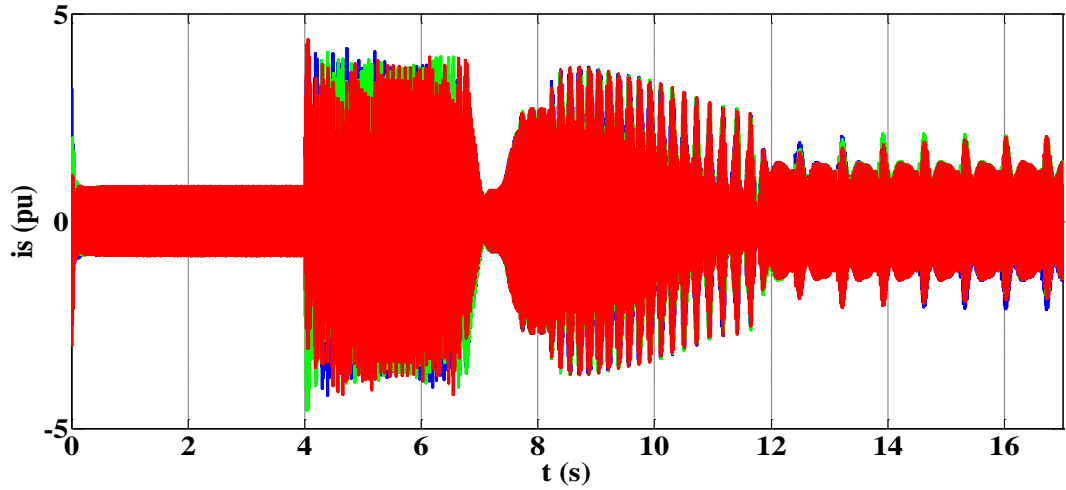
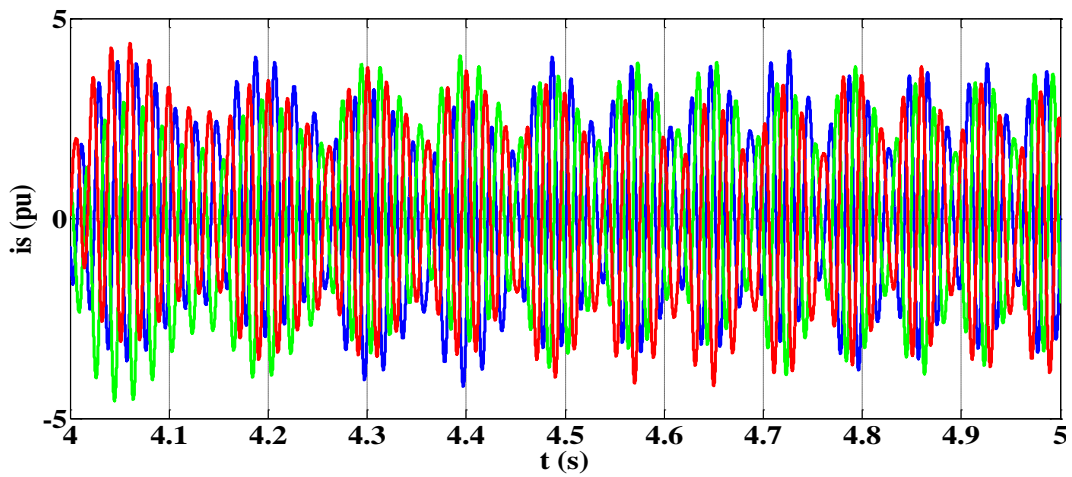


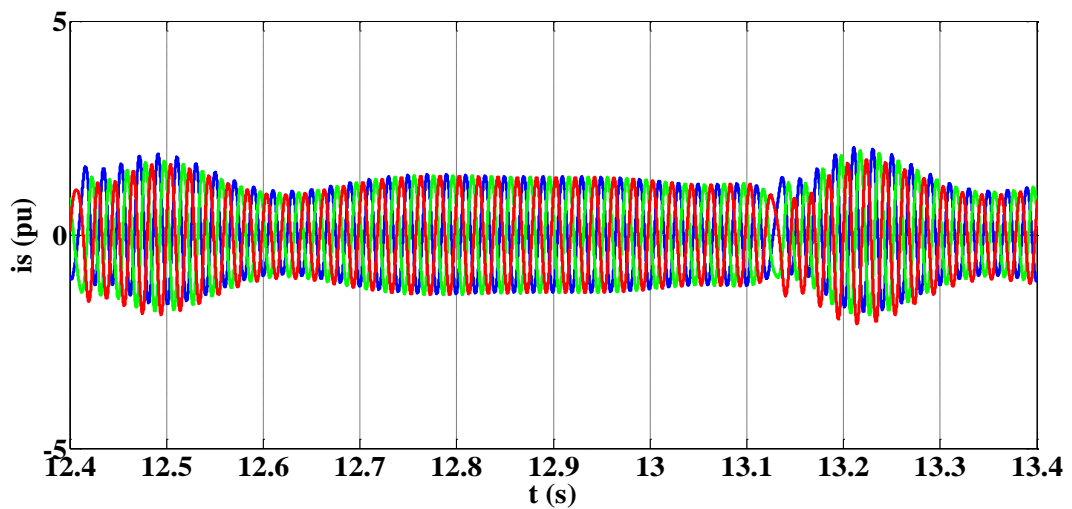
Figure 11. Rotor currents (short-circuit happens at  $t = 4$  s).



(a)

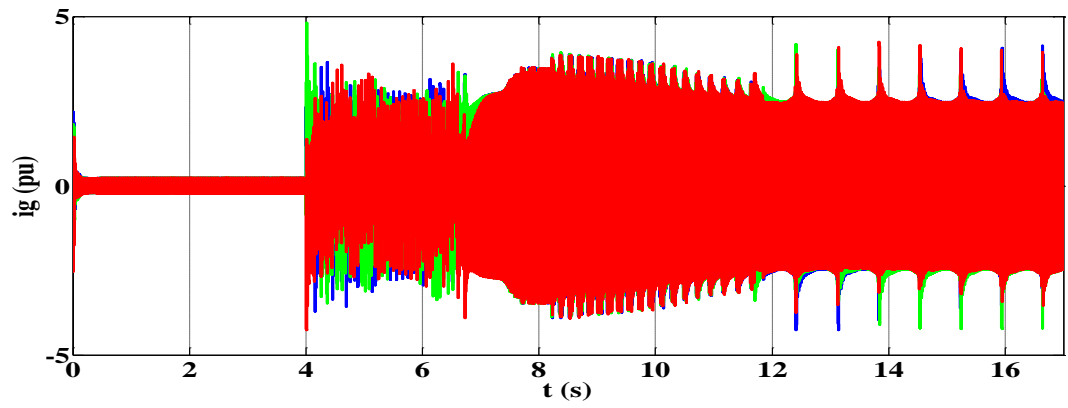


(b)

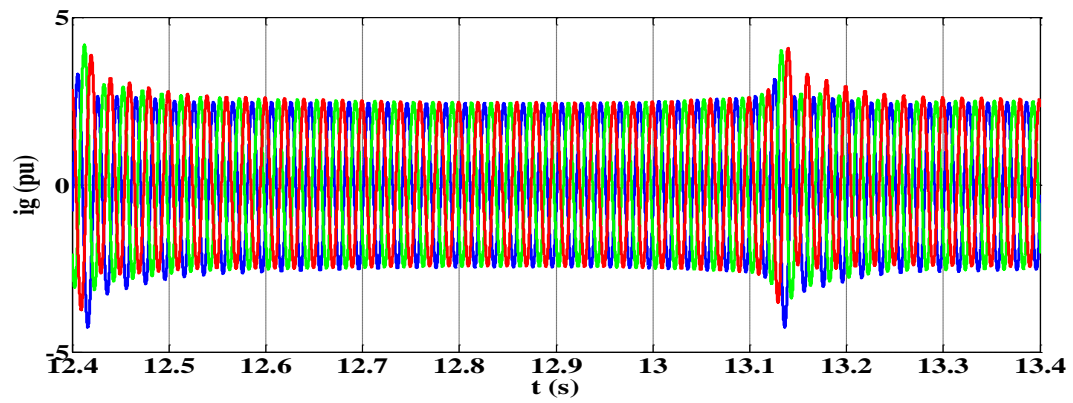


(c)

**Figure 12.** (a) Stator currents (short-circuit happens at  $t = 4$  s), (b) zoom of (a) immediately after fault; (c) zoom of (a) after system equilibrates.

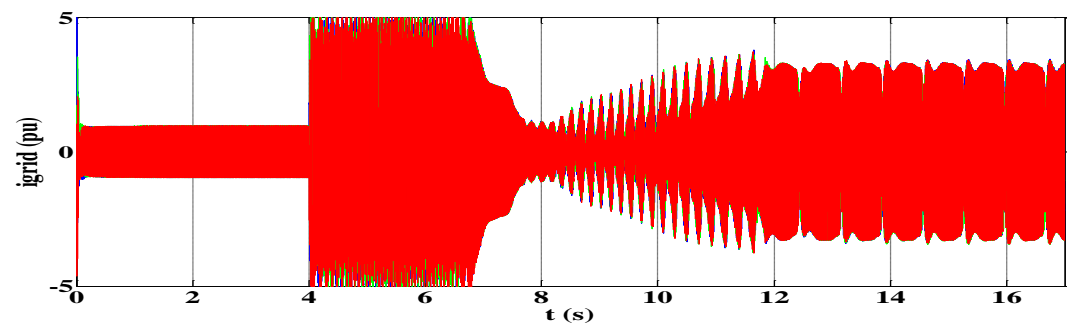


(a)

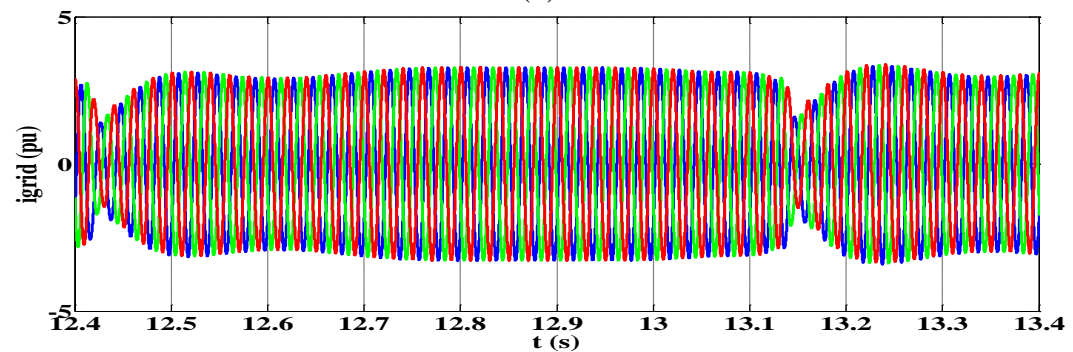


(b)

**Figure 13.** (a) Grid Side Converter (GSC) phase currents  $I_{gabc}$  (short-circuit happens at  $t = 4$  s), (b) zoom of (a).



(a)



(b)

**Figure 14.** (a) Grid phase currents  $I_{gridabc}$  (short-circuit happens at  $t = 4$  s), (b) zoom of (a).

From everything mentioned before, one can easily conclude that the consequences of a short-circuit fault in one IGBT of RSC will be catastrophic for the system, so an adequate control and a protection system must be adopted for fault clearance, system protection during fault and possible DFIG disconnection. Using current measurements (e.g., rotor phase currents that are measured in any way) and when a threshold has been exceeded a command to interrupt the IGBTs pulsating must be given.

#### 4.2. Short-Circuit in One IGBT of the GSC (F2)

In this case the DFIG reaction under (F2)—Figure 1—Is investigated. DFIG has been operated in supersynchronous mode ( $n_r = 1800 \text{ rpm} > n_s = 1500 \text{ rpm}$ —Synchronous speed) and at  $t = 4 \text{ s}$  a short-circuit occurred in T1 (upper IGBT, phase a). As in previous case, no change in IGBTs pulsation has been considered during the simulation, except for IGBT (1), which has been short-circuited (GSC phase current  $i_{ga}$  and currents through T1, T4 (IGT1, IGT4) that have been affected by (F2), are shown in Figure 15, where very high current peak values can also be observed). The protection system has been considered not to be activated and the system has reached in a steady faulty state. Take in account the simulation results one can see that (F2) affects the operational behavior of the whole system and the consequences of this kind of fault are similar to the corresponding ones of fault (F1), but a little slighter. Initially, the transient phenomenon lasts less than that in case of (F1) (from  $t = 4 \text{ s}$  to  $t = 10 \text{ s}$ ). The electromagnetic torque oscillation is smaller than the previous case, so the danger for mechanical part breakdown is lower (Figure 16). Rotor speed  $n_r$  (rpm) (Figure 17) increases to 2200 rpm (pitch control could be possibly activated, but due to the fact that it consists of mechanical parts, it has high time constant) and finally decreases at 1530 rpm (smoother reaction than under (F1)). Also, pulsations appear in stator active power. Figure 18 shows that (F2) has a high impact on the dc link voltage as it decreases significantly and becomes almost zero. Both rotor (Figure 19) and stator (Figure 20) currents are affected by (F2). More specifically, a dc component and very high peak values appear in stator currents—Approximately 3.5 times the nominal value during the transient condition and 1.8 times after system equilibration (different and smoother reaction than under (F1)), while rotor currents get high values. Finally, in Figures 21 and 22 one can see that both GSC line currents  $I_{gabc}$  and grid phase currents  $I_{gridabc}$  get high peak values (3.5–4 times the nominal value) and a dc component also appears, that could cause saturation or damage in the grid-side filter and the transformer.

As in the previous case one can conclude that an adequate control and a protection system must be adopted for fault clearance, system protection during fault and possible DFIG disconnection. As in previous case a way to protect the system is measuring rotor phase currents, comparing their values with a threshold and when it has been exceeded a command to interrupt the IGBTs pulsating must be given.

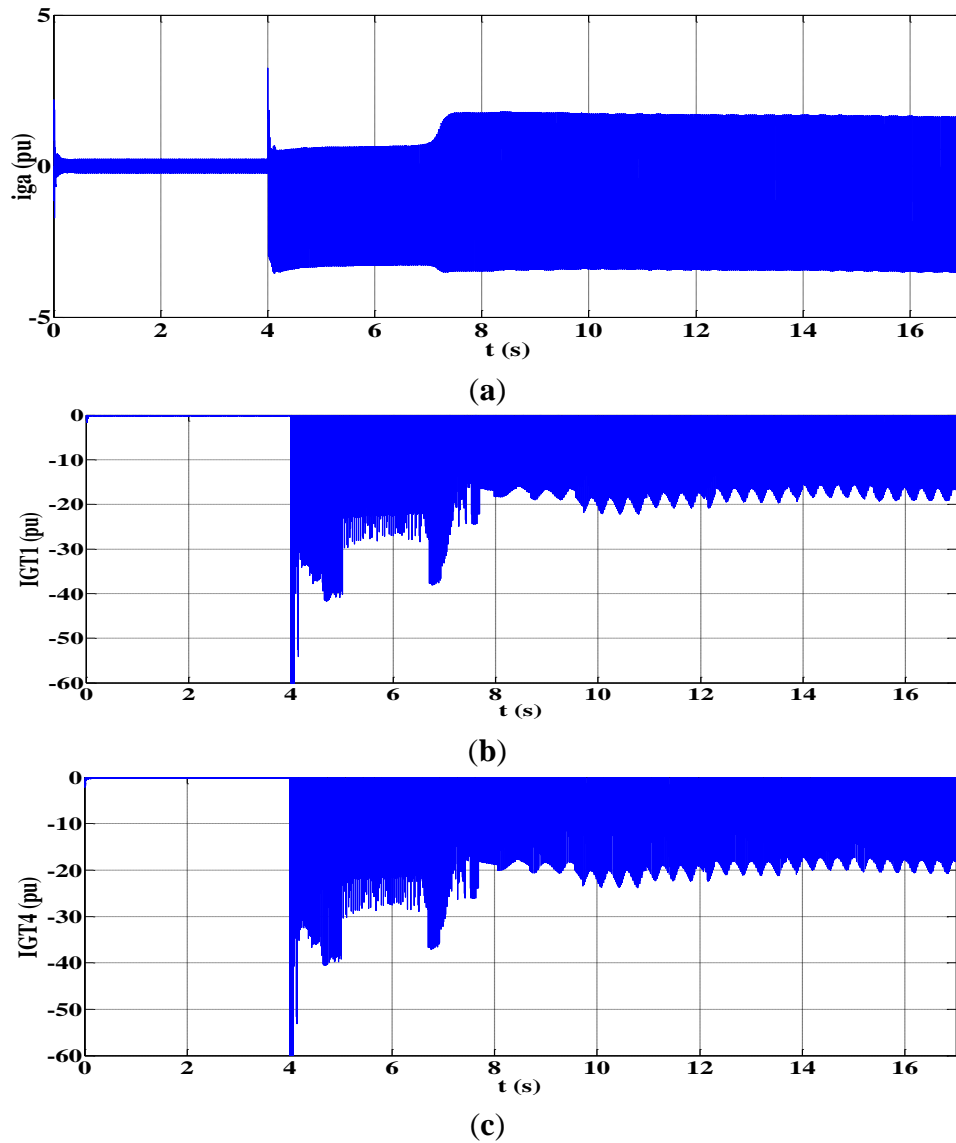


**Figure 15.** Waveforms of the characteristic variables of the Grid Side Converter (GSC): (a) Grid Side Converter (GSC) phase current  $i_{ga}$ , (b) Current through Insulated Gate Bipolar Transistor (IGBT) (1), (c) Current through Insulated Gate Bipolar Transistor (IGBT) (4) (short-circuit happens at  $t = 4$  s for all waveforms).

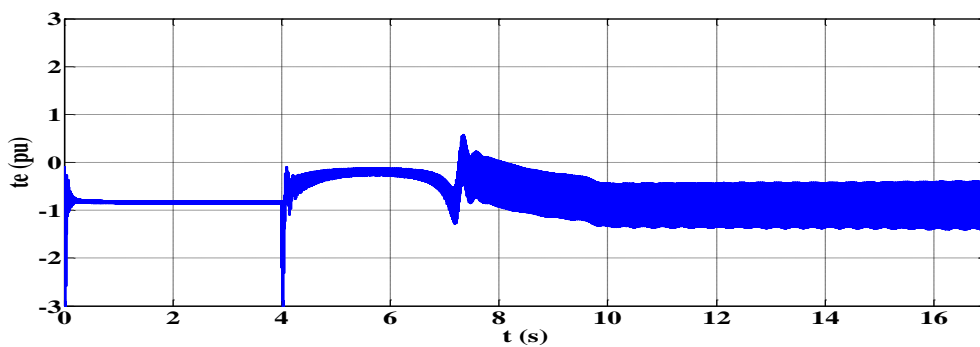


**Figure 16.** Electromagnetic torque (short-circuit happens at  $t = 4$  s).

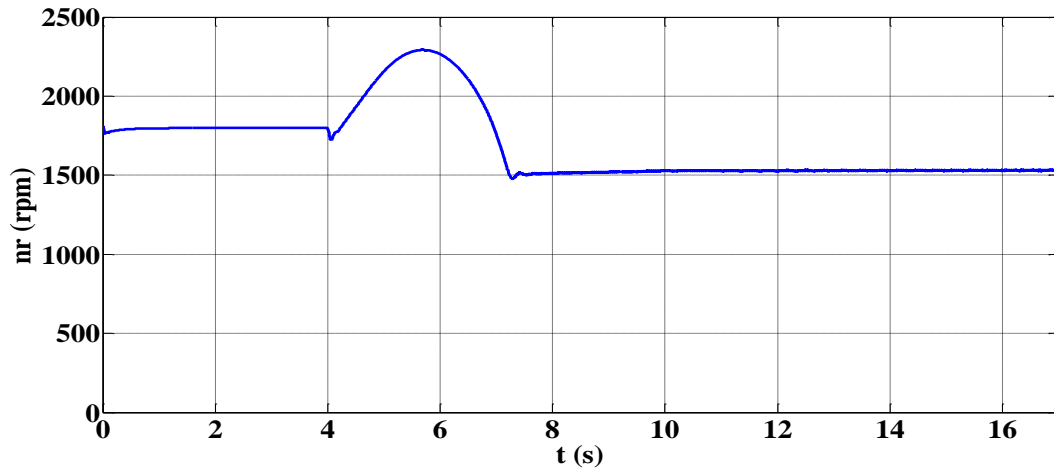


Figure 17. Rotor speed  $n_r$  (short-circuit happens at  $t = 4$  s).

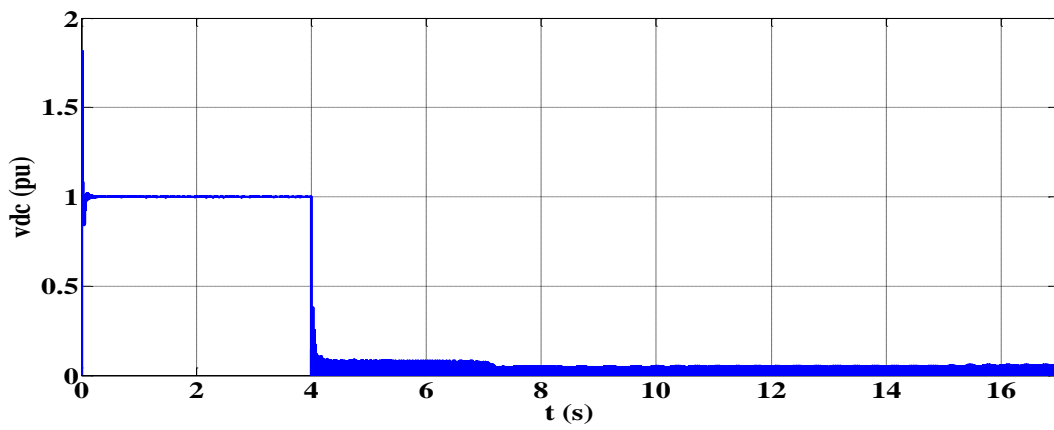


Figure 18. DC link voltage (short-circuit happens at  $t = 4$  s).

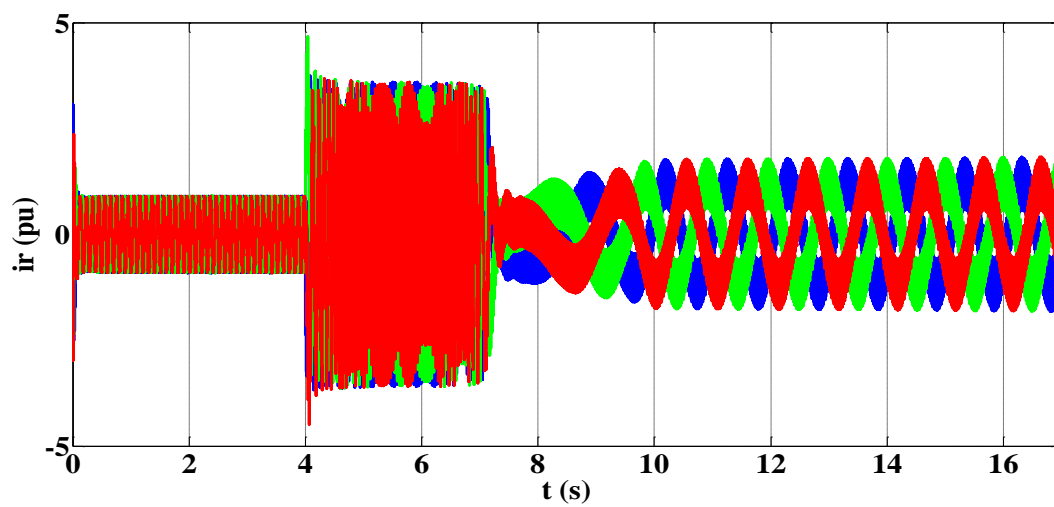
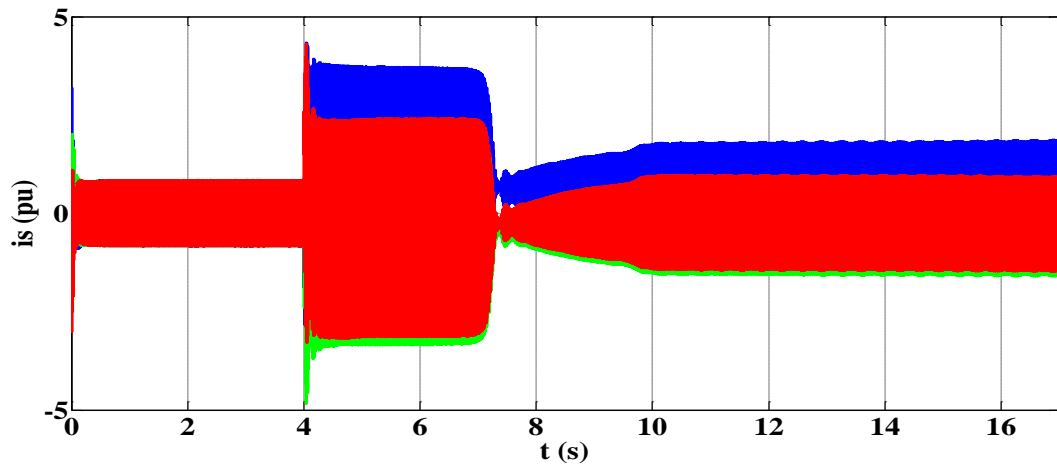
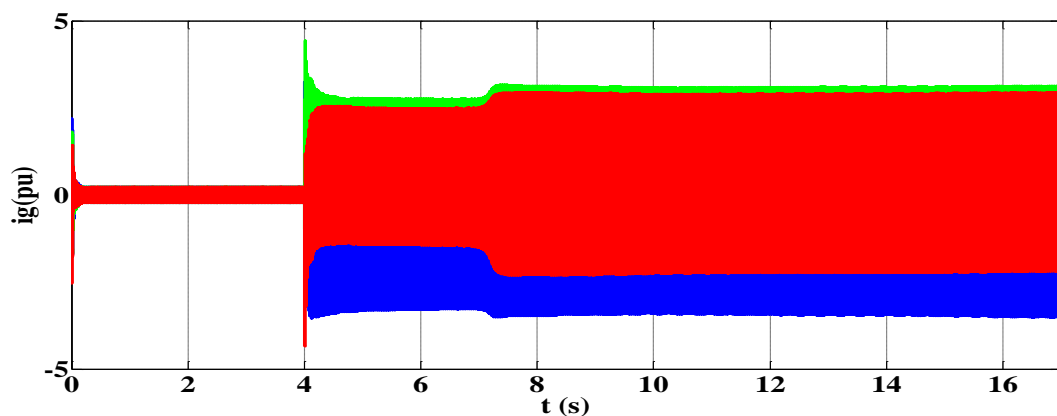


Figure 19. Rotor currents (short-circuit happens at  $t = 4$  s).



**Figure 20.** Stator currents (short-circuit happens at  $t = 4$  s).



**Figure 21.** Grid Side Converter (GSC) phase currents  $I_{gabc}$  (short-circuit happens at  $t = 4$  s).

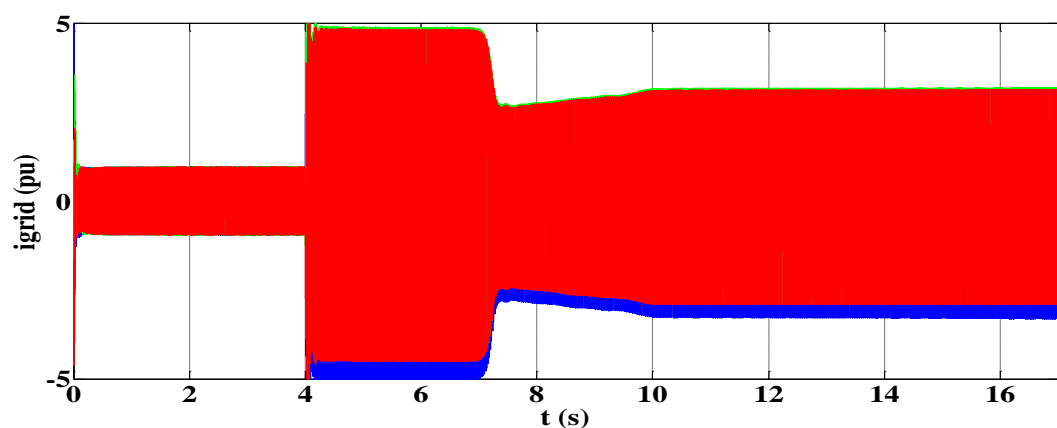


**Figure 22.** Grid phase currents  $I_{gridabc}$  (short-circuit happens at  $t = 4$  s).

#### 4.3. Short-Circuit in Two Rotor Terminals (Phase-to-Phase Short-Circuit) (F3)

In this section the DFIG behavior under fault (F3)—Figure 1—is studied. DFIG has been operated in supersynchronous mode ( $n_r = 1800$  rpm  $>$   $n_s = 1500$  rpm—Synchronous speed) and at  $t = 4$  s short-circuit occurred in two rotor terminals—Phase-to-phase short-circuit (b, c). The protection system has been considered not to be activated and the system has reached in a steady faulty state. Initially, a

slight transient phenomenon happens, which lasts for a time interval of 2 s (from  $t = 4$  s to  $t = 6$  s). A pulsating torque ( $t_e$ ) has been caused (Figure 23) with great low frequency oscillations and has as a result severe vibration on the mechanical part of the system (turbine-generator-gearbox) and maybe total breakdown of the system (similar to the corresponding one under (F1)-Figure 7). Rotor speed  $n_r$  (Figure 24) decreases and oscillates at 1570 rpm ( $\pm 30$  rpm). Furthermore, pulsations appear in stator active power, which is no more regulated and this could cause problems to the grid. Figure 25 shows that (F3) has a high effect on the dc link voltage as it decreases significantly. Both rotor (Figure 26) and stator (Figure 27) currents are affected by (F3). More specifically, very high peak values appear in rotor currents—approximately four times the nominal value during the transient condition and two times after system equilibration—and a high harmonic content appears. Stator currents get high values and a high harmonic content appears too. Finally, in Figures 28 and 29 one can see that (F3) causes a great increase of the peak value (3.5–4 times the nominal value) and oscillations in both GSC line currents  $I_{gabc}$  and grid phase currents  $I_{gridabc}$ .

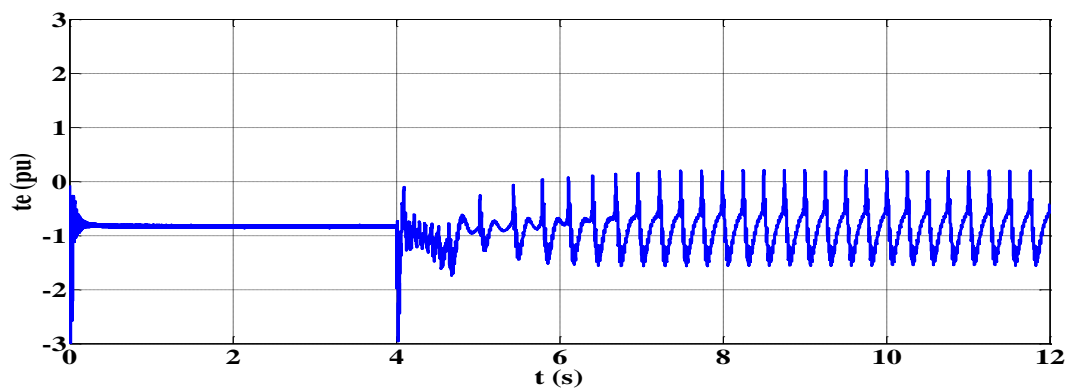


**Figure 23.** Electromagnetic torque (short-circuit happens at  $t = 4$  s).

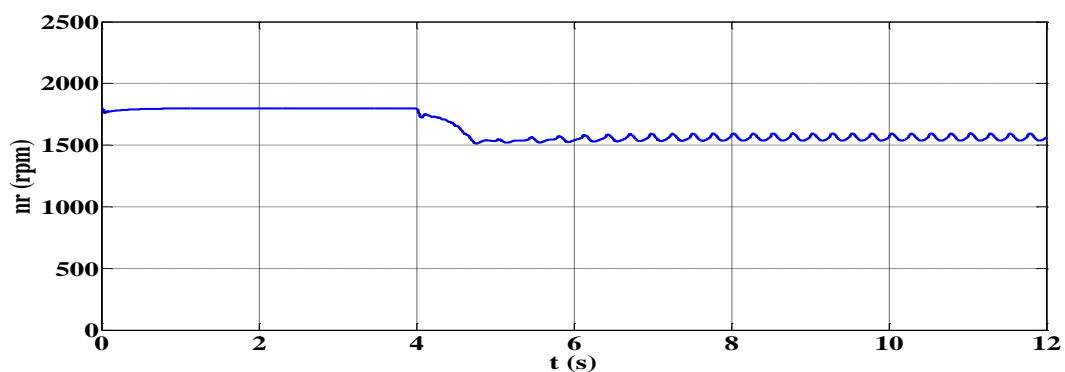


**Figure 24.** Rotor speed  $n_r$  (short-circuit happens at  $t = 4$  s).

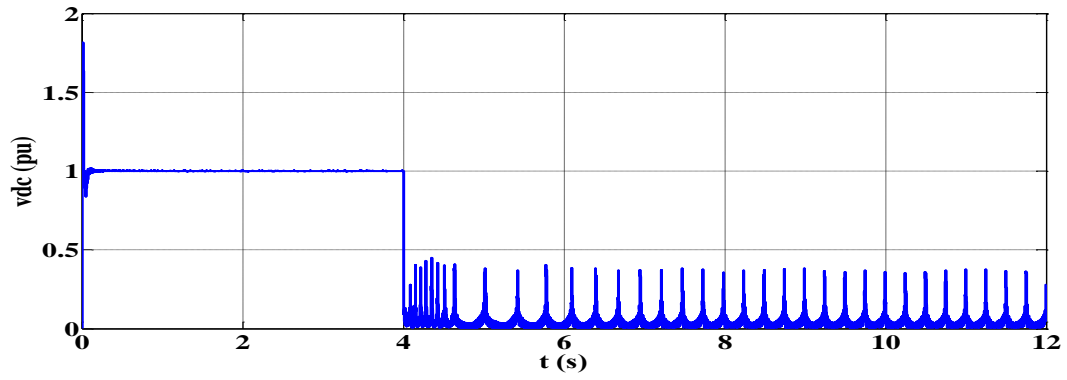


Figure 25. DC link voltage (short-circuit happens at  $t = 4$  s).

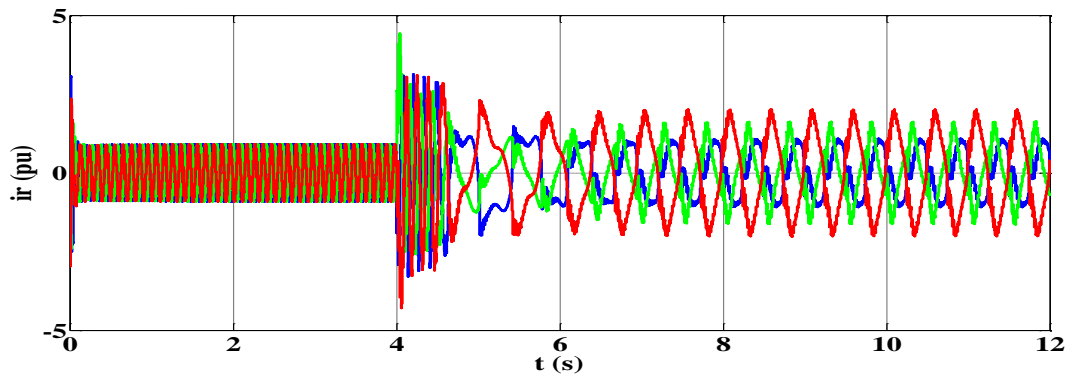
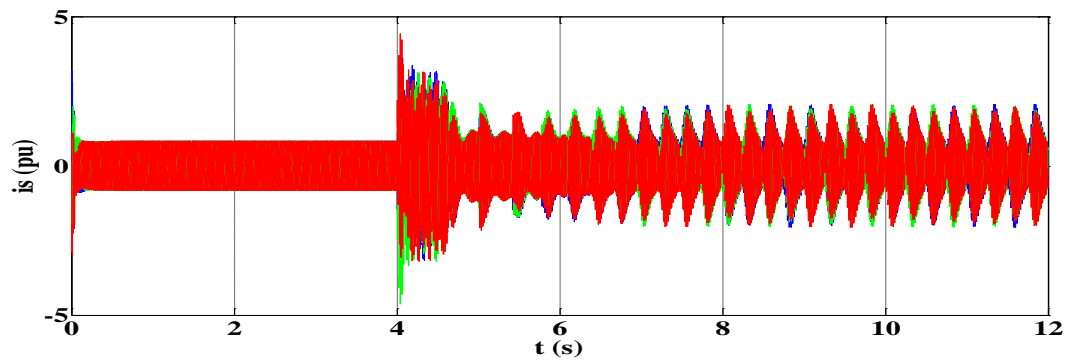
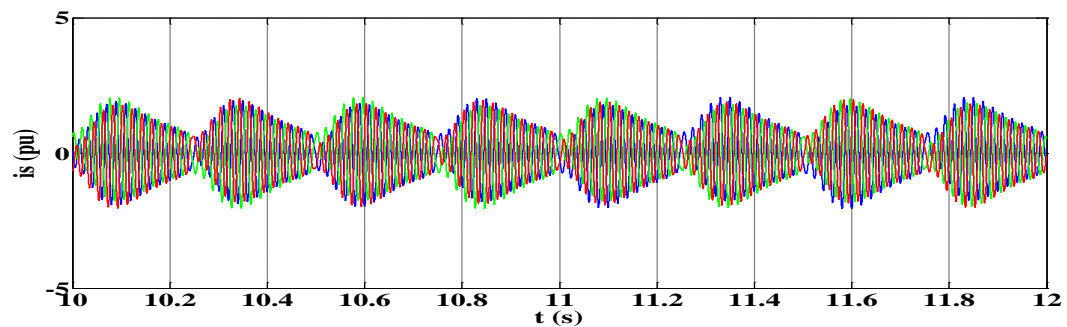


Figure 26. Rotor currents (short-circuit happens at  $t = 4$  s).

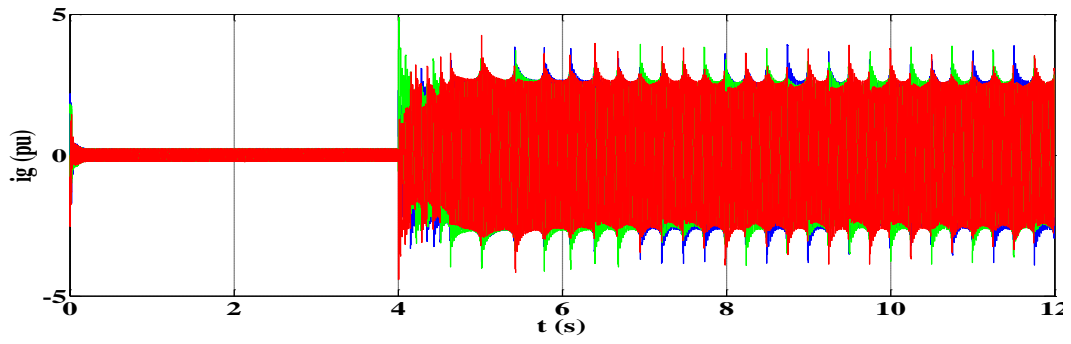


(a)

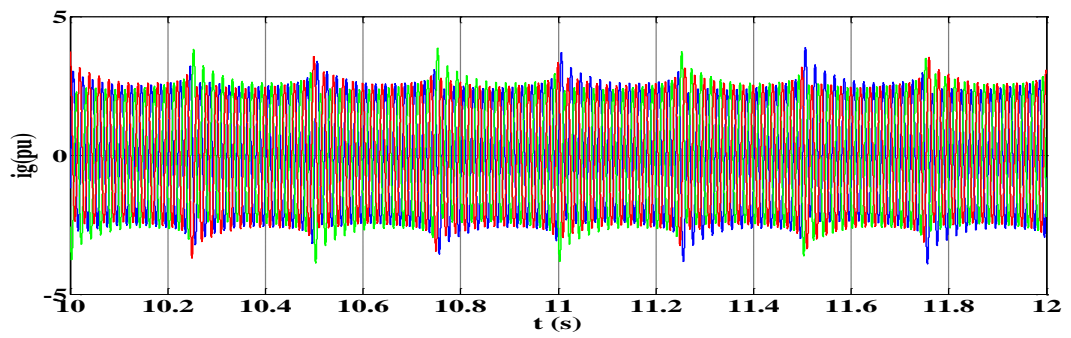


(b)

Figure 27. (a) Stator currents (short-circuit happens at  $t = 4$  s), (b) zoom of (a).

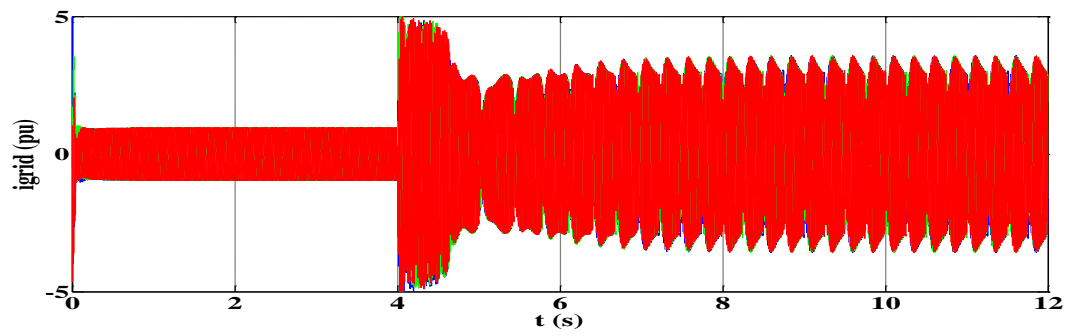


(a)

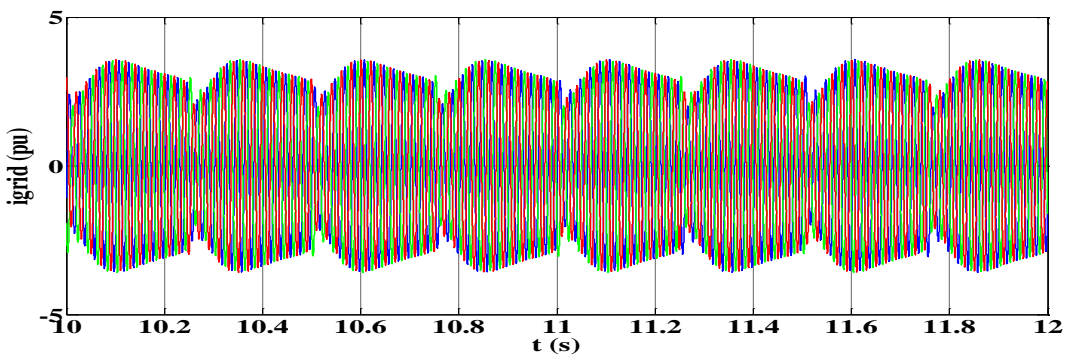


(b)

Figure 28. (a) GSC line currents (short-circuit happens at  $t = 4$  s), (b) zoom of (a).



(a)



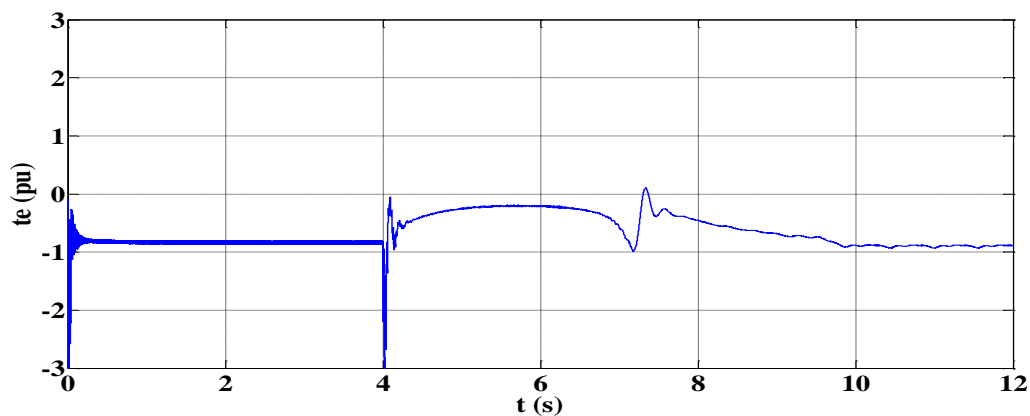
(b)

Figure 29. (a) Grid line currents (short-circuit happens at  $t = 4$  s), (b) zoom of (a).

As it is also concluded for this case, a specific control and a protection system must be considered to face possible problems to system operation. Both generator windings and converter electronic power switches danger to be damaged (along with the mechanical part of DFIG due to strong oscillations).

#### 4.4. Short-Circuit in Three Rotor Terminals (Three Phase Short-Circuit) (F4)

In this section the DFIG behavior under fault (F4)—Figure 1—is studied. DFIG has been operated in supersynchronous mode ( $n_r = 1800 \text{ rpm} > n_s = 1500 \text{ rpm}$ —Synchronous speed) and at  $t = 4 \text{ s}$  a short-circuit occurred in three rotor terminals—three phase short-circuit. The protection system has been considered not to be activated and the system has reached in a steady faulty state. Initially, a large (larger than during (F3)) transient phenomenon happens, which lasts for a time interval of 6 s (from  $t = 4 \text{ s}$  to  $t = 10 \text{ s}$ ). The torque pulsations are not as great as under (F3) (Figure 30) so the mechanical part of the system (turbine-generator-gearbox) is not suffered from such strong vibrations. Rotor speed  $n_r$  (rpm) (Figure 31) decreases at 1527 rpm (very close to synchronous speed). Figure 32 shows that (F4) has a high effect on the dc link voltage as it decreases significantly. Both rotor (Figure 33) and stator (Figure 34) currents are affected by (F4). More specifically, very high peak values appear—approximately four times the nominal value during the whole transient condition, which lasts for a long time, and 1.5 times after system equilibration. Finally, in Figures 35 and 36 one can see that (F4) causes a great increase of the peak value (3.5–4 times the nominal value) and oscillations in both GSC line currents  $I_{gabc}$  and grid phase currents  $I_{gridabc}$ .



**Figure 30.** Electromagnetic torque (short-circuit happens at  $t = 4 \text{ s}$ ).

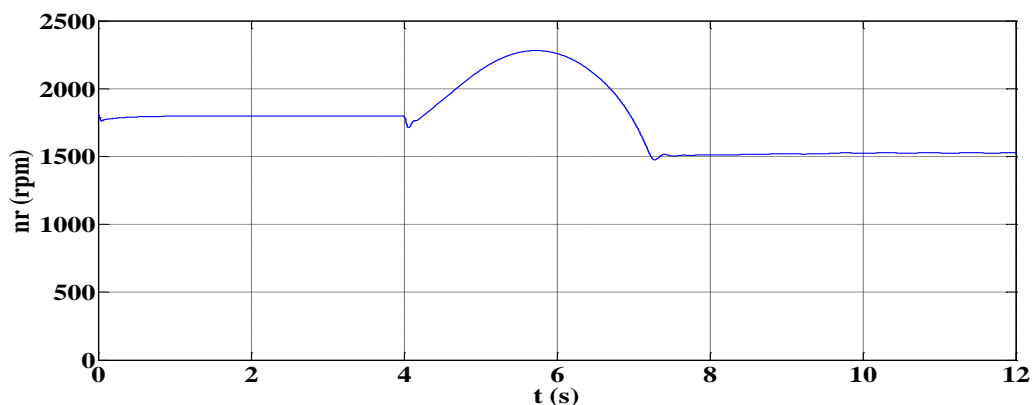


**Figure 31.** Rotor speed  $n_r$  (short-circuit happens at  $t = 4 \text{ s}$ ).

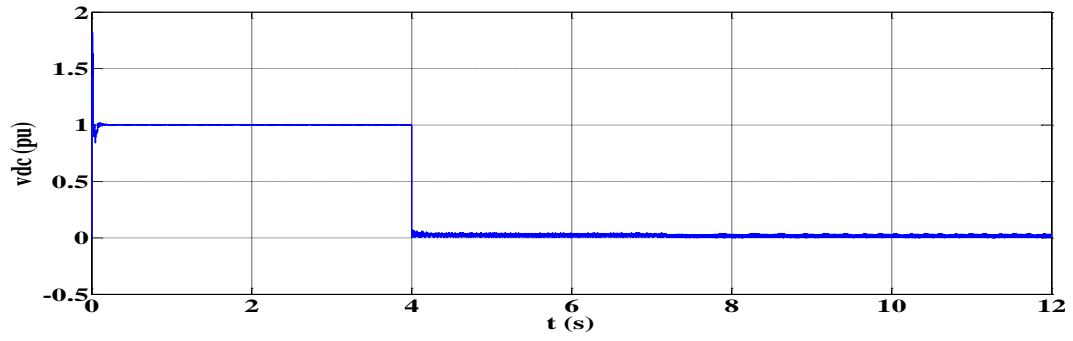


Figure 32. DC link voltage (short-circuit happens at  $t = 4$  s).

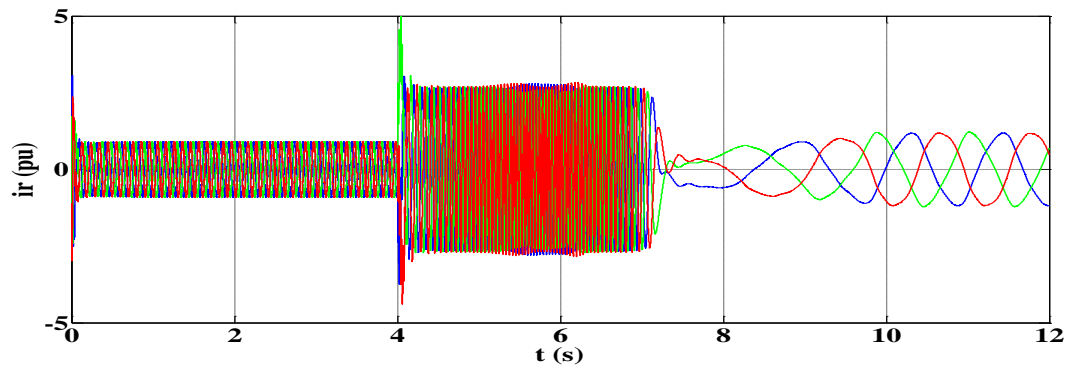
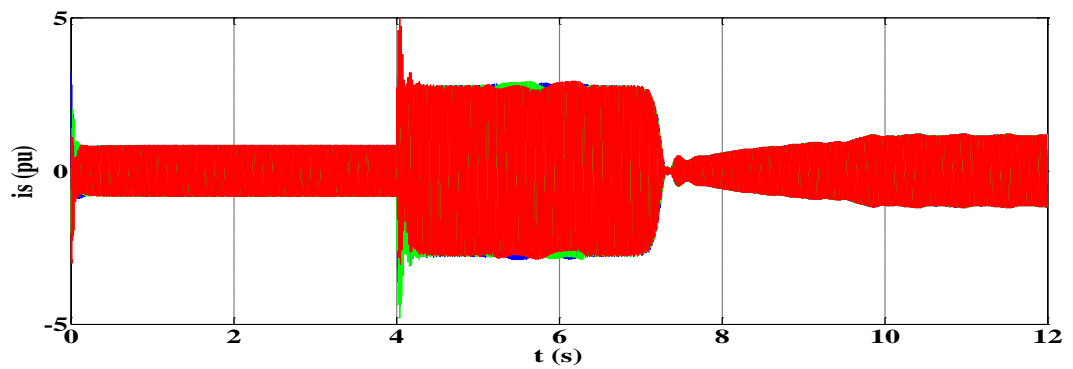
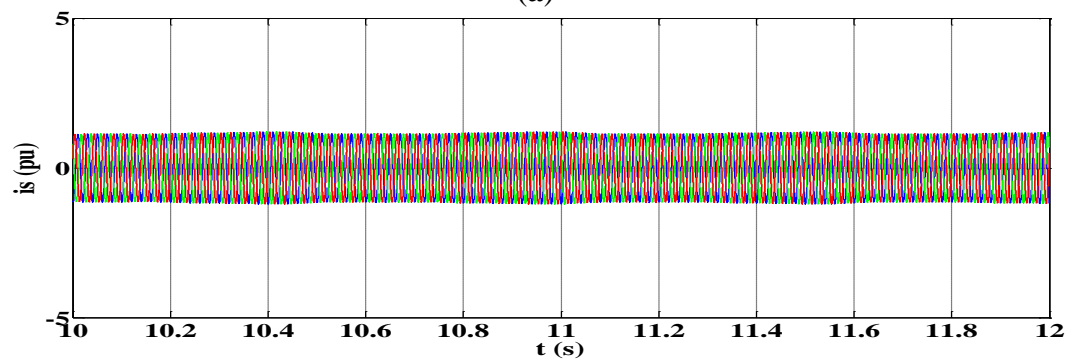


Figure 33. Rotor currents (short-circuit happens at  $t = 4$  s).

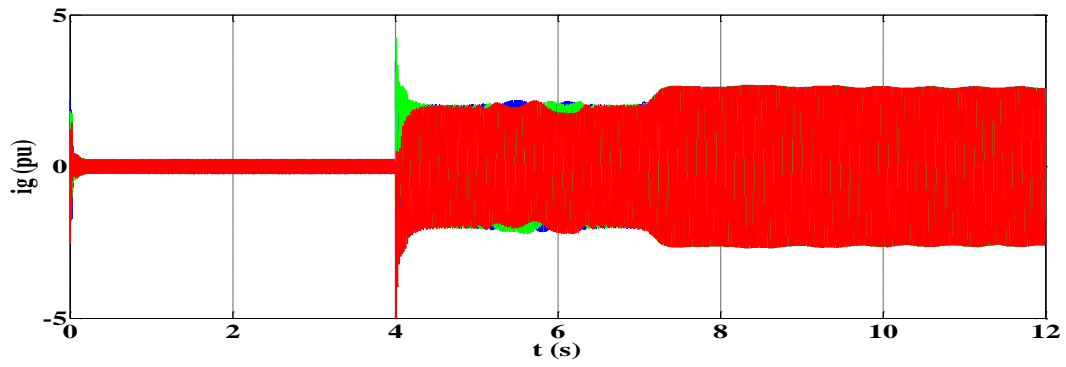


(a)

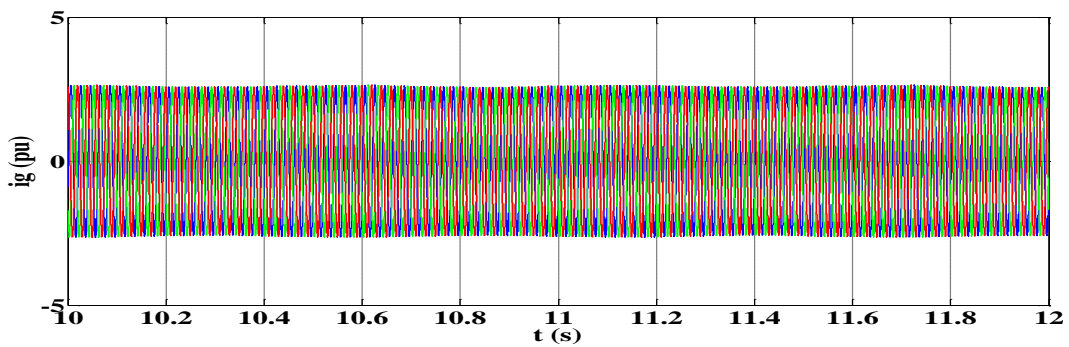


(b)

Figure 34. (a) Stator currents (short-circuit happens at  $t = 4$  s), (b) zoom of (a).

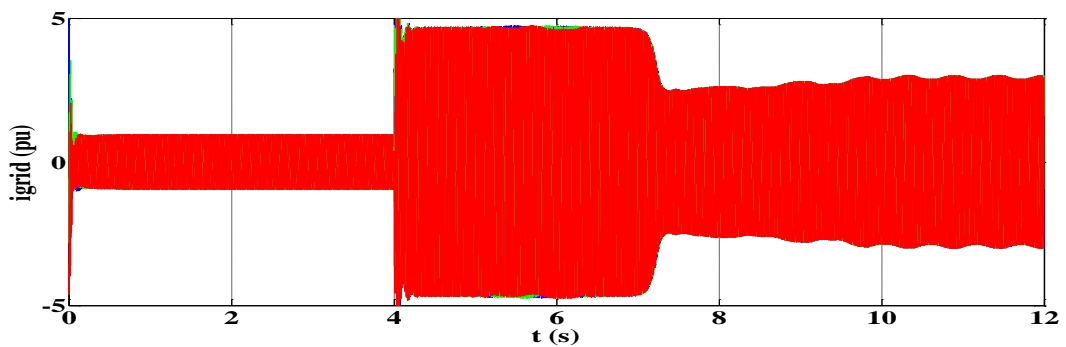


(a)

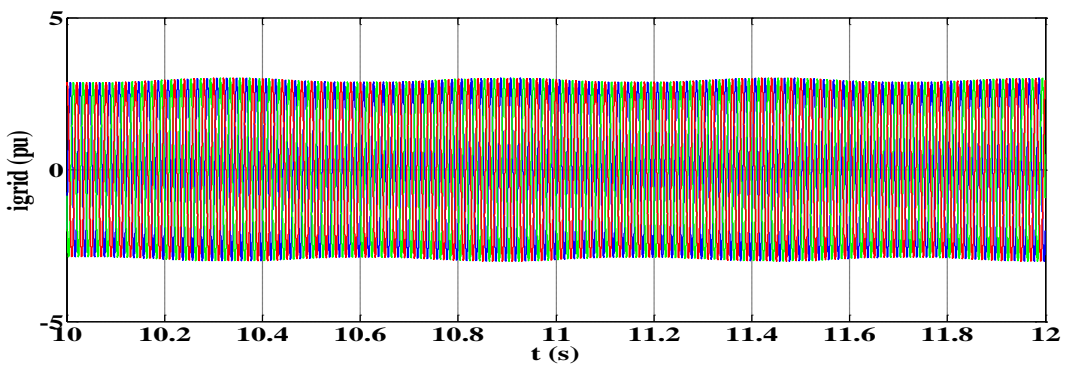


(b)

**Figure 35.** (a) Grid Side Converter (GSC) line currents (short-circuit happens at  $t = 4$  s), (b) zoom of (a).



(a)



(b)

**Figure 36.** (a) Grid line currents (short-circuit happens at  $t = 4$  s), (b) zoom of (a).

As it has been concluded from the above results both generator windings and converter electronic power switches danger to be damaged due to the high currents peak values, but in this case the vibrations of the mechanical part are slighter.

## 5. Conclusions

In this paper short-circuit in one IGBT of the back-to-back converter and a phase-to-phase short-circuit in the terminals of rotor have been considered and DFIG-WECS behavior has been investigated. From simulation results, one can conclude that a short-circuit in one IGBT of RSC affects the whole system. More specifically, a pulsating torque has been caused with great low frequency oscillations and results a severe vibration on the mechanical part of the system (turbine-generator-gearbox) and maybe total breakdown of the system. Moreover, rotor speed decreases at 1555 rpm (very close to synchronous speed and with oscillations  $\pm 40$  rpm). Pulsations also appear in stator active power, which is no more regulated and this could cause problems to the grid. This fault has a high effect on the dc link voltage as it decreases significantly. Furthermore, both rotor and stator currents are strongly affected. More specifically, a dc component and very high peak values appear in rotor currents—Approximately four times the nominal value during the transient condition and 1.3 times after system equilibration, while stator currents get high values. The dc component worsens the current stress of the healthy converter switches (especially in supersynchronous mode). However, rotor windings and the converter switches could be damaged during the transient state.

In case that a short-circuit fault occurs in one IGBT of GSC, a slight transient phenomenon happens. Torque oscillations have been also caused and rotor speed decreases and oscillates at 1530 rpm (very close to synchronous speed). DC link voltage becomes almost to zero in this case. A dc component and very high peak values appear in stator currents—Approximately 3.5 times the nominal value during the transient condition and 1.8 times after system equilibration (different and smoother reaction than the previous case), while rotor currents get high values. GSC line currents and grid phase currents get high peak values (3.5–4 times the nominal value) and a dc component also appears, that could cause saturation or damage in the grid-side filter and the transformer.

Subsequently, when a phase-to-phase short-circuit happens in rotor terminals, a pulsating torque also appears, which may cause severe vibration on the mechanical part of the system (turbine-generator-gearbox) and maybe total breakdown of the system (similar to the corresponding one in the first case). Rotor speed oscillates at 1570 rpm (close to synchronous speed). Furthermore, pulsations appear in stator active power, which is no more regulated and this could cause problems to the grid. Both rotor and stator currents are affected by this fault. More specifically, very high peak values appear in rotor currents—approximately four times the nominal value during the transient condition and two times after system equilibration—and a high harmonic content appears. Stator currents get high values and a high harmonic content appears too. The DFIG reaction in this specific faulty condition is similar to that when a short-circuit fault happens in one IGBT of RSC.

Finally, when a three phase short-circuit happens in rotor terminals, the most serious consequence is the increase of the machine and back-to-back electronic converter currents, which could cause damages to both machine windings and converter electronic power switches. In all cases investigated in this paper, it is clearly concluded that an adequate control and a protection system must be considered to face the

problems to system operation, because both generator windings and converter power switches danger to be damaged, along with the mechanical part of DFIG due to strong torque oscillations. So, a possible operation principle of a protection system could be using current measurements (e.g., rotor phase currents that are measured anyway, so there would be no additional cost) and when a threshold has been exceeded, a command to interrupt the IGBTs pulsating must be given for system shutdown.

### Author Contributions

Dimitrios G. Giaourakis has been responsible for the whole system modeling and simulation in Matlab/Simulink. Athanasios N. Safacas has been responsible for the evaluation of the simulation results.

### Conflicts of Interest

The authors declare no conflict of interest.

### References

1. Tchakoua, P.; Wamkeue, R.; Ouhrouche, M.; Slaoui-Hansaoui, F.; Tameghe, T.A.; Ekemb, G. Wind turbine condition monitoring: State-of-the-art review, new trends, and future challenges. *Energies* **2014**, *7*, 2595–2630.
2. Tsili, M.; Papathanassiou, S. A review of grid code technical requirements for wind farms. *IET Renew. Power Gener.* **2009**, *3*, 308–332.
3. Lopez, J.; Sanchis, P.; Roboam, X.; Marroyo, L. Dynamic behavior of the doubly fed induction generator during three-phase voltage dips. *IEEE Trans. Energy Convers.* **2007**, *22*, 709–717.
4. Marquez, G.D.; Sousa, D.M. Understanding the doubly fed induction generator during voltage dips. *IEEE Trans. Energy Convers.* **2012**, *27*, 421–431.
5. Arribas, J.R.; Rodriquez, A.F.; Munoz, A.H.; Nicolas, C.V. Low voltage ride-through in DFIG wind generators by controlling the rotor current without crowbars. *Energies* **2014**, *7*, 498–519.
6. Zheng, Z.; Yang, G.; Geng, H. Coordinated control of a doubly-fed induction generator-based wind farm and a static synchronous compensator for low voltage ride-through grid code compliance during asymmetrical grid faults. *Energies* **2013**, *6*, 4660–4681.
7. Blaabjerg, F.; Liserre, M.; Ma, K. Power electronic converters for wind turbine systems. *IEEE Trans. Ind. Appl.* **2012**, *48*, 708–719.
8. Ribrant, J.; Bertling, L.M. Survey of failures in wind power systems with focus on Swedish wind power plants during 1997–2005. *IEEE Trans. Energy Convers.* **2007**, *22*, 167–173.
9. Hahn, B.; Durstewitz, M.; Rohrig, K. Reliability of wind turbines: Experiences of 15 years with 1500 WTs. *Wind Energy* **2007**, *10*, 329–332.
10. Mensah, A.F.; Duenas-Osorio, L. A closed-form technique for the reliability and risk assessment of wind turbine systems. *Energies* **2012**, *5*, 1734–1750.
11. Shah, D.; Nandi, S.; Neti, P. Stator-interturn-fault detection of doubly fed induction generators using rotor-current and search-coil-voltage signature analysis. *IEEE Trans. Ind. Appl.* **2009**, *45*, 1831–1842.

12. Boulkroune, B.; Galvez-Carillo, M.; Kinnaert, M. Combined signal and model-based sensor fault diagnosis for a doubly fed induction generator. *IEEE Trans. Control Syst. Technol.* **2013**, *21*, 1771–1783.
13. Rothenhagen, K.; Fuchs, F.W. Doubly fed induction generator model-based sensor fault detection and control loop reconfiguration. *IEEE Trans. Ind. Electron.* **2009**, *56*, 4229–4238.
14. Giaourakis, D.; Safacas, A.; Tsotoulidis, S. Dynamic behaviour of a wind energy conversion system including doubly-fed induction generator in fault conditions. *Int. J. Renew. Energy Res.* **2012**, *2*, 219–226.
15. Karimi, S.; Gaillard, A.; Poure, P.; Saadate, S. FPGA-based real-time power converter failure diagnosis for wind energy conversion systems. *IEEE Trans. Ind. Electron.* **2008**, *55*, 4299–4308.
16. Duan, P.; Xie, K.-G.; Zhang, L.; Rong, X. Open-switch fault diagnosis and system reconfiguration of doubly fed wind power converter used in a microgrid. *IEEE Trans. Power Electron.* **2011**, *26*, 816–821.
17. Khomfoi, S.; Kok, W.S.; Ngamroo, I. An open circuit fault diagnostic technique in IGBTs for AC to DC converters applied in microgrid applications. *J. Power Electron.* **2011**, *11*, 801–810.
18. Giaourakis, D.G.; Safacas, A.; Tsotoulidis, S. Start-up behaviour of the Doubly-Fed Induction generator in a wind energy conversion system. In Proceedings of the 2013 IEEE International Conference on Renewable Energy Research and Applications (ICRERA), Madrid, Spain, 21–23 October 2013; pp. 127–132.
19. Giaourakis, D.G.; Safacas, A. Response of doubly-fed induction generator wind energy conversion system in dynamic situations-wind, grid and converter perturbations. In Proceedings of the 2014 IEEE International Conference on Electrical Machines (ICEM), Berlin, Germany, 2–5 September 2014.
20. Nanou, S.; Tsourakis, G.; Vournas, C.D. Full-converter wind generator modeling for transient stability studies. In Proceedings of the 2011 IEEE Trondheim PowerTech, Trondheim, Norway, 9–23 June 2011; pp. 1–7.
21. Lu, B.; Sharma, S.K. A literature review of IGBT fault diagnostic and protection methods for power inverters. *IEEE Trans. Ind. Appl.* **2009**, *45*, 1770–1777.

© 2015 by the authors; licensee MDPI, Basel, Switzerland. This article is an open access article distributed under the terms and conditions of the Creative Commons Attribution license (<http://creativecommons.org/licenses/by/4.0/>).